JPhys Photonics

PAPER • OPEN ACCESS

# Broadband multi-longitudinal-mode Yb:YAG/$YVO_4$ coupled Raman microchip laser

IOP Publishing J. Phys. Photonics 2 (2020) 045007 https://doi.org/10.1088/2515-7647/abac1b

Journal of Physics: Photonics

OPEN ACCESS

RECEIVED
7 May 2020

REVISED
21 July 2020

ACCEPTED FOR PUBLICATION
4 August 2020

PUBLISHED
2 September 2020



PAPER

# Broadband multi-longitudinal-mode Yb:YAG/$YVO_4$ coupled Raman microchip laser

**Xihao Qiao, Peng Sun, Xiaolei Wang, Hanjie Wang and Jun Dong**

Laboratory of Laser and Applied Photonics (LLAP), Department of Electronic Engineering, School of Electronic Science and Engineering, Xiamen University, Xiamen 361005, People's Republic of China

**E-mail:** jdong@xmu.edu.cn

**Keywords:** microchip laser, Raman laser, multi-longitudinal modes, coupled cavity

## Abstract

Broadband lasers oscillating in multiple longitudinal modes have potential applications on high resolution interferometer, optical communication and laser spectroscopy. However, the bandwidth of the laser spectrum is limited by the spectral range of laser materials. Here, a broadband multi-longitudinal-mode laser with bandwidth of 22.4 nm at first-order Stokes wavelength has been achieved in a Yb:YAG/$YVO_4$ Raman microchip laser pumped with a quasi-continuous-wave laser-diode. The output energy is 11.6 mJ at pump energy of 34.4 mJ, and the optical efficiency is 34%. Dramatically expanding multi-longitudinal-mode laser spectrum has been achieved by forming Yb:YAG/$YVO_4$ coupled Raman microchip laser with an external Fabry–Perot mirror to manipulate the output coupling losses at different frequencies for fundamental, first-order and second-order Stokes lasers. The bandwidth of the broadband multi-longitudinal-mode laser is 55.4 nm, which covers from 1041 nm to 1096.4 nm and includes 118 longitudinal modes. This enables compact coupled Raman microchip solid-state lasers for generating broadband multi-longitudinal-mode laser.

## 1. Introduction

Multiple wavelength lasers (MWL) have been widely used in wavelength division multiplexed communication [1], optical sensing [2], high resolution laser interferometer [3], medical sensing [4], nonlinear frequency conversion [5], nonlinear dynamic [6], terahertz generation [7] and so on. Various methods have been proposed for developing MWLs. Extra optical elements have been inserted in the laser cavity for generating MWLs, different emission lines of laser crystals have been utilized to achieve MWLs by controlling the cavity length and the coating for different laser lines [8, 9]. MWLs have been demonstrated with different laser gain media [10]. The optical parametric oscillator has been used to generate MWL [11]. However, extra optical elements, special coating designing and special laser cavity design for maintaining phase matching make these laser systems complex and cost. Therefore, it is greatly desirable for developing compact, robust and stable miniature lasers for generating MWLs. The multi-longitudinal-mode is a large number of discrete frequencies determined by the axial modes oscillating in a laser cavity. The multi-longitudinal modes oscillating in a Fabry–Perot microchip laser are determined by the cavity length, gain bandwidth of the gain medium and pump power. The broadband multi-longitudinal-mode laser can be achieved by applying high pump power. Multi-longitudinal-mode operation of semiconductor lasers has been widely used in multiplexed optical communications, and is also desirable for generating high output power or energy [12]. However, applications are limited by the low beam quality of semiconductor lasers and extra beam shaping elements needed to couple laser beams. Laser-diode end-pumped solid-state microchip lasers have been demonstrated for generating high beam quality multi-longitudinal-mode laser and suitable for generating wide laser spectrum by using laser media with broad emission spectrum. Multi-longitudinal mode oscillation in Yb:YAG microchip laser has been observed owing to the broad emission spectrum of Yb:YAG crystal [13, 14]. However, the lasing spectral range obtained in the crystalline lasers is restricted by the spontaneous fluorescence emission bandwidth of laser gain materials. Fortunately, the stimulated Raman

scattering (SRS) effect of Raman gain media has been used to expand the laser spectral bandwidth in the solid-state Raman lasers. Since the CW self-Raman laser was demonstrated with an Nd:KGW crystal as a working medium [15], many new wavelength lasers has been developed based on Nd:$YVO_4$, Nd:KGW/KGW, Nd:$GdVO_4$, $BaWO_4$ and diamond Raman crystals [16–20]. The effective output coupling is not spectrally and spatially uniform for the fundamental field in the Raman laser. The spectrally varied output coupling loss for the fundamental field has been utilized for expanding laser spectrum in the intracavity Raman lasers. Multi-colour lasers with selectable wavelengths in the visible and near-infrared regions have been experimentally demonstrated by using an Nd:$GdVO_4$ crystal [21]. Compared to the narrow emission spectra of the $Nd^{3+}$-ions doped crystals, $Yb^{3+}$-ions doped crystals such as Yb:YAG with broad emission spectra have more advantages for generating broad laser spectra and efficient performance have been demonstrated in microchip lasers and ultra-fast lasers [22]. Passively Q-switched self-Raman lasers have been developed by using Yb:$KGd(WO_4)_2$ [23], Yb:$KY(WO_4)_2$ [24] and Yb:$YVO_4$ [25] crystals. However, severe thermal loading of self-Raman lasers limits the output power because self-Raman crystals work as gain medium and Raman medium simultaneously. The gain and loss for the fundamental and Raman laser fields are difficult to be balanced simultaneously in self-Raman lasers, thus, it is a challenge for achieving efficient self-Raman lasers. Therefore, optimization of the laser crystal and Raman crystal separately in an intracavity Raman laser becomes more effective for developing efficient Raman lasers. Yb:YAG crystal has been successfully used for constructing passively and actively Q-switched Raman lasers with $YVO_4$ crystal as Raman medium [26, 27]. Yb:YAG and Nd:$YVO_4$ crystals have been used to construct Raman microchip laser (RML) oscillating at 1050 nm, 1080 nm and 1123 nm multiple wavelengths [28]. Expansion of the lasing spectral range has been demonstrated in a monolithic $YVO_4$-Nd:$YVO_4$ self-mode-locked Raman laser [29], passively mode-locked fiber lasers with few-layer bismuthene [30], topological insulator [31] as saturable absorber, a passively mode-locked erbium-doped fiber laser with large anomalous-dispersion [32], and a whispering-gallery mode cavity [33]. Further expansion of the lasing spectral range upon to 8.4 THz has been achieved in a self-mode-locked Yb:KGW Raman laser with an external Fabry–Perot (FP) cavity [34]. Broadband multi-longitudinal-mode laser with a bandwidth of 7.64 nm has been obtained in a Yb:YAG/$YVO_4$ RML [35]. However, further expansion of the laser spectrum in Yb:YAG/$YVO_4$ RML was limited because the thermal effect of Yb:YAG crystal was aggravated at high pump power. It is well known that efficient operation of Yb:YAG lasers at ambient temperature can be achieved with high pump power intensity [36]. Thermal effect in solid-state lasers can be alleviated by using quasi-continuous-wave (QCW) laser diodes as pump sources. The high pump power intensity can be achieved by applying high power QCW laser diode. Therefore, with QCW laser diode as a pump source, further expansion of the bandwidth of the multi-longitudinal-mode laser should be expected in a Yb:YAG/$YVO_4$ coupled-RML with an external coupled cavity.

Here, efficient, broadband multi-longitudinal-mode Raman lasers have been demonstrated in a QCW laser diode pumped Yb:YAG/$YVO_4$ RMLs with different $YVO_4$ crystal length ($l_R$). Optical efficiency of 34% and multi-longitudinal-mode Raman laser with spectral bandwidth of 22.4 nm have been achieved in the RML with $l_R = 1.5$ mm. Further expansion of bandwidth of the multi-longitudinal-mode laser has been achieved in a Yb:YAG/$YVO_4$ coupled-RML formed with an external FP cavity. The broadband multi-longitudinal-mode laser is from 1041 nm to 1096.4 nm, which includes 118 longitudinal modes. The bandwidth is more than 55.4 nm. The experimentally obtained broadband multi-longitudinal-mode laser is in good agreement with the theoretically calculated results based on Raman conversion from fundamental laser at 1050 nm with two Raman shift lines of 259 $cm^{-1}$ and 155 $cm^{-1}$.

## 2. Experiments

Raman microchip laser (RML) cavity, as shown in figure 1(a), consists of a conventional Fabry–Perot (F-P) resonator with a highly doped Yb:YAG crystal as the gain medium and a *c*-cut $YVO_4$ crystal as the Raman gain medium. The F-P resonator was formed with high reflection mirror (M1) and output mirror (M2) directly coated on the Yb:YAG and $YVO_4$ crystals. A $\phi 10 \times 1.2$ mm Yb:YAG crystal doped with 15 at.% $Yb^{3+}$ ions was used as laser gain medium. Highly doped $Yb^{3+}$:YAG crystal is favorable for laser oscillation at 1050 nm. Anti-reflection (AR) at 940 nm and high-reflection (HR) at 1030–1100 nm were coated on one surface of Yb:YAG crystal to form the rear mirror of the cavity (M1). The Raman gain media were three undoped *c*-cut $YVO_4$ crystals with thickness ($l_R$) of 1, 1.5 and 2 mm, respectively. HR was coated on one surface of the $YVO_4$ crystal to serve as front cavity mirror (M2). The transmission spectrum of M2 on $YVO_4$ crystal was shown in figure 1(b). The enlarged transmission spectrum of M2 was shown in the inset of figure 1(b). The transmission (T) at 1030 nm, 1050 nm were 0.6%, 0.5%, while the T was about 0.3% from 1060 nm to 1100 nm. And the T was about 0.6% around 1120 nm. AR at 1030–1200 nm was coated on the facing surfaces of the Yb:YAG and $YVO_4$ crystals to reduce the intracavity losses. A high power fiber-coupled quasi continuous-wave (QCW) laser-diode oscillating at 940 nm was used as pump source to achieve high

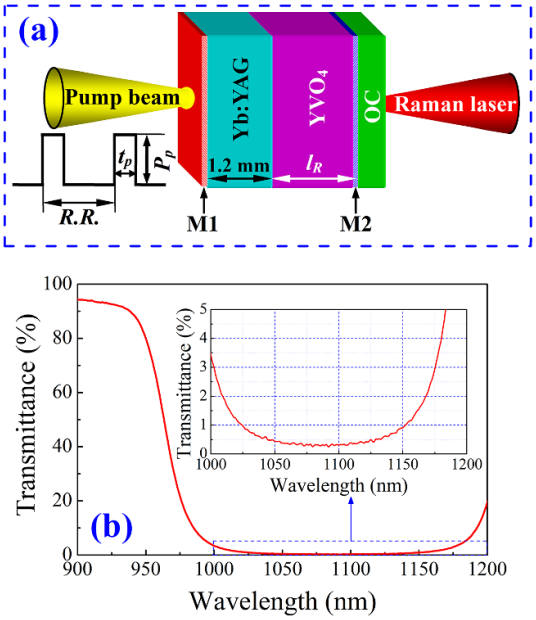


**Figure 1.** (a) Schematic diagram for QCW laser diode pumped Yb:YAG/$YVO_4$ RMLs. M1 is the rear cavity mirror, M2 is the front cavity mirror, $l_R$ is the length of the $YVO_4$ crystal, $t_p$, $P_p$, and *R.R.* are the pulse duration, pump power and repetition rate of QCW laser diode, respectively. (b) Transmission spectrum of the coating M2 on $YVO_4$ crystal, inset is the enlarged transmission spectrum of M2 from 1000 to 1200 nm.

pump power intensity and alleviate the thermal effect of RML. The core diameter of the fiber is 200 $\mu$m and the numerical aperture is 0.22. Two lenses with focal length of 8 mm were used to collimate and focus pump beam. The focused beam diameter is 160 $\mu$m. The output laser from QCW laser-diode is square pulsed laser with pump power ($P_p$), pump pulse duration ($t_p$) and pump repetition rate ($R.R$). The maximum $P_p$ can be reached to 100 W. The $t_p$ was set to 0.9 ms in the experiment. The *R.R.* was set to 10 Hz. No active cooling system was used in the laser experiment operating at room temperature. An optical spectral analyzer (Anritsu, MS9740A) was used to analyze the lase spectra of the Yb:YAG/$YVO_4$ RMLs with three $l_R$s. The resolution of the optical spectral analyzer is 0.03 nm. The generated lasers were focused with a lens (100 mm focal length), then coupled into a multimode fiber that connected the optical spectral analyzer. The average output powers of RMLs and coupled RML were measured with a Thorlabs power meter. Then the output energies of the lasers were obtained by dividing the average output power by repetition rate of the lasers (10 Hz).

## 3. Results

### 3.1. Yb:YAG/$YVO_4$ RML

Firstly, the performance of QCW laser-diode pumped Yb:YAG/$YVO_4$ RMLs with three $l_R$s was investigated. An optical spectral analyzer (Anritsu, MS9740A) was used to analyze the lase spectra of the Yb:YAG/$YVO_4$ RMLs with three $l_R$s. Figure 2 depicts the some typical laser emitting spectra of the Yb:YAG/$YVO_4$ RMLs with three $l_R$s at different $P_{in}$s. Multi-longitudinal modes were dominant for the fundamental lasers and Raman lasers, which were induced by the broad emission spectrum of Yb:YAG crystal around 1.05 $\mu$m [13]. The longitudinal mode number and spectral bandwidth increase with $P_{in}$.

For Yb:YAG/$YVO_4$ RML with $l_R = 1$ mm, as shown in figure 2(a), the laser oscillated at 1050 nm fundamental wavelength and 1079 nm Raman wavelength when the $P_{in}$ was 3.1 W. The first-order Stokes laser at 1079 nm was generated from the fundamental laser at 1050 nm with Raman shift line at 259 $cm^{-1}$. The Raman laser at 1079 nm oscillated simultaneously with the fundamental laser at 1050 nm as $P_{in}$ increases. The longitudinal modes of the fundamental and first-order Stokes laser increased with $P_{in}$, one example at $P_{in} = 3.1$ W and 12.5 W was shown in figure 2(a). When the $P_{in}$ reached 18 W, another fundamental laser oscillated at 1030 nm. The intensity of 1030 nm fundamental laser increases and the intensity of 1050 nm fundamental laser decreases with increase in $P_{in}$, this is caused by the competition of two fundamental lasers for the laser gain. The laser spectral range was dramatically expanded for the first-order Stokes laser at 1079 nm at $P_{in} = 24.5$ W. Further increasing $P_{in}$ up to 38.3 W, three lasers at 1030 nm, 1050 nm, and 1079 nm oscillated simultaneously except some variation of the intensities. The bandwidth is 15 nm for the first-order Raman laser covering from 1072 nm to 1087 nm. There are 31

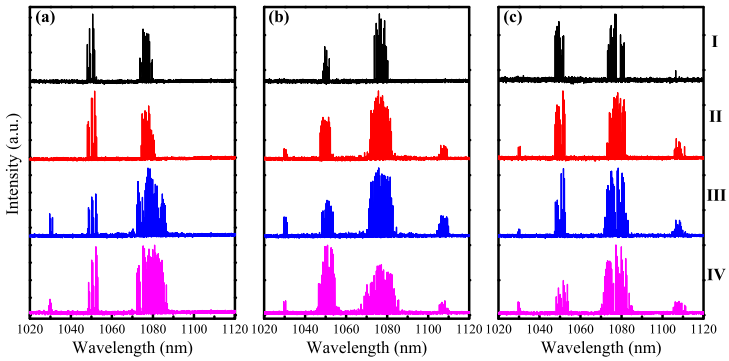


**Figure 2.** Laser spectra of Yb:YAG/$YVO_4$ RMLs. (a) Laser spectra of Yb:YAG/$YVO_4$ RMLs with $l_R = 1$ mm at different input pump powers (I: $P_{in} = 3.1$ W, II: $P_{in} = 12.5$ W, III: $P_{in} = 24.5$ W, IV: $P_{in} = 38.3$ W). (b) Laser spectra of RML with $l_R = 1.5$ mm at different $P_{in}$s (I: $P_{in} = 3.1$ W, II: $P_{in} = 12.5$ W, III: $P_{in} = 24.5$ W, IV: $P_{in} = 38.3$ W). (c) Laser spectra of RML with $l_R = 2$ mm at different $P_{in}$s (I: $P_{in} = 3.1$ W, II: $P_{in} = 12.5$ W, III: $P_{in} = 24.5$ W, IV: $P_{in} = 38.3$ W).

longitudinal modes at $P_{in} = 38.3$ W. The excitation of fundamental laser at 1030 nm was attributed to increased loss at 1050 nm due to generation of the first-order Stokes laser with 259 $cm^{-1}$ Raman shift line from 1050 nm fundamental laser. The generation of Raman laser from fundamental laser at 1050 nm can be treated as an enhanced loss for fundamental laser at 1050 nm. With increase in $P_{in}$, the gain accumulated at 1030 nm fundamental laser increased, while the loss at 1030 nm was not changed. Therefore, the gain at 1030 nm provided with high pump power exceeds the reabsorption loss and supports oscillation of the 1030 nm fundamental laser. This phenomenon is similar to the oscillation of the 1063 nm and 1066 nm dual-wavelength laser obtained in high power pumped Nd:$GdVO_4$ self-Raman laser [18].

When the $YVO_4$ crystal length increased to 1.5 mm, as shown in figure 2(b), the fundamental and Raman lasers oscillated simultaneously at 1050 nm and 1079 nm respectively at $P_{in} = 3.1$ W, which was similar to that for the Yb:YAG/$YVO_4$ RML with $l_R = 1$ mm. Dual-wavelength laser oscillation was kept until the $P_{in}$ increased to 7 W. When the $P_{in}$ was higher than 7 W, the second-order Stokes laser oscillated at 1110 nm. The cascade Raman conversion with 259 $cm^{-1}$ Raman shift line is responsible for generating second-order Stokes laser from the first-order Stokes laser at 1079 nm. The first-order Stokes field at 1079 nm was enhanced with increase of $P_{in}$. Thus, the intracavity Raman laser intensity at 1079 nm was increased sufficient to overcome the lasing threshold of the second-order Stokes laser. The laser spectra at 1050 nm, 1079 nm and 1110 nm expanded with further increasing in $P_{in}$. One more fundamental laser oscillated at 1030 nm when the $P_{in}$ was higher than 11 W. Therefore, four-wavelength laser oscillated simultaneously at 1030 nm, 1050 nm, 1079 nm and 1110 nm, as shown in figure 2(b) at $P_{in} = 12.5$ W (II). With further increase in the $P_{in}$, four-wavelength laser was kept except the intensity, and bandwidth of the laser spectra expanded, as shown in figure 2(b) at $P_{in} = 25.4$ W (III) and 2(b) at $P_{in} = 38.3$ W (IV). The first-order Stokes laser spectral bandwidth is 22.4 nm covering from 1063.17 nm to 1085.57 nm and including 44 longitudinal modes at $P_{in} = 38.3$ W. The spectral bandwidth of the 1050 nm fundamental laser is 11.7 nm covering from 1045.64 nm to 1057.34 nm and including 23 longitudinal modes. There are 3 longitudinal modes around 1030 nm and there are 9 longitudinal modes around 1108 nm (from 1105.46 nm to 1110.23 nm).

Further increase the $YVO_4$ Raman crystal length to 2 mm, the laser spectrum of the Yb:YAG/$YVO_4$ RML at $P_{in} = 3.1$ W is different from those obtained in RML with $l_R = 1$ mm and 1.5 mm. The RML with $l_R = 2$ mm oscillated at 1050 nm (fundamental laser), 1079 nm (first-order Stokes laser) and 1106 nm (second-order Stokes laser), as shown in figure 2(c) at $P_{in} = 3.1$ W (I). When $P_{in}$ was increased to 5 W, another fundamental laser oscillated at 1030 nm. Therefore, four-wavelength laser at 1030, 1050, 1079 and 1108.5 nm oscillated simultaneously, as shown in figure 2(c) at $P_{in} = 12.5$ W (II) and $P_{in} = 25.4$ W (III). When the $P_{in}$ was increased to 38.3 W, the multi-longitudinal-mode first-order Stokes laser covered from 1069.88 nm to 1085.15 nm, the bandwidth was 15.27 nm including 31 longitudinal modes. The fundamental laser at 1050 nm oscillates in multi-longitudinal modes, and the bandwidth is 5.9 nm covering from 1048.17 nm to 1054.07 nm and including 13 longitudinal modes. The second-order Raman laser also oscillates in multi-longitudinal modes, the bandwidth is 5.92 nm covering from 1105.31 nm to 1111.23 nm and including 15 longitudinal modes. Table 1 summaries the spectra of the multi-longitudinal-mode lasers obtained in three Yb:YAG/$YVO_4$ RMLs with different $l_R$s at $P_{in} = 38.3$ W. From table 1 and figure 2, we can see that the widest spectral bandwidth of 22.4 nm has been obtained for the first-order Stokes laser generated in the RML with $l_R = 1.5$ mm.

**Table 1.** Laser spectral properties of Yb:YAG/$YVO_4$ RMLs with different $l_R$s at $P_{in}$ = 38.3 W.

| $l_R$ (mm) | | 1 | 1.5 | 2 |
|---|---|---|---|---|
| Wavelength (nm) | $\lambda_{F1}$ | 1030 | 1030 | 1030 |
| | $\lambda_{F2}$ | 1050 | 1050 | 1050 |
| | $\lambda_{S1}$ | 1079 | 1079 | 1079 |
| | $\lambda_{S2}$ | – | 1110 | 1110 |
| Laser spectral range (nm) | $\lambda_{F1}$ | 1029.36–1030.26 | 1029.57–1030.47 | 1029.62–1030.52 |
| | $\lambda_{F2}$ | 1048.18–1053.07 | 1045.64–1057.34 | 1048.17–1054.07 |
| | $\lambda_{S1}$ | 1072.24–1087.03 | 1063.17–1085.57 | 1069.88–1085.15 |
| | $\lambda_{S2}$ | – | 1105.46–1110.23 | 1105.31–1111.23 |
| Spectral bandwidth, $\Delta\lambda$ (nm) | $\lambda_{F1}$ | 0.9 | 0.9 | 0.92 |
| | $\lambda_{F2}$ | 4.89 | 11.7 | 5.9 |
| | $\lambda_{S1}$ | 14.79 | 22.4 | 15.27 |
| | $\lambda_{S2}$ | – | 4.8 | 5.92 |
| Longitudinal modes | $\lambda_{F1}$ | 3 | 3 | 3 |
| | $\lambda_{F2}$ | 11 | 23 | 13 |
| | $\lambda_{S1}$ | 30 | 44 | 31 |
| | $\lambda_{S2}$ | – | 9 | 15 |

Notes: $\lambda_{F1}$ is the wavelength of the fundamental laser at 1030 nm, $\lambda_{F2}$ is the wavelength of the fundamental laser at 1050 nm, $\lambda_{S1}$ is the wavelength of the first-order Stokes Raman laser at 1079 nm, $\lambda_{S2}$ is the wavelength of the second-order Stokes Raman laser at 1110 nm, $\Delta\lambda$ is the spectral bandwidth of generated laser around fundamental and Stokes lasers.

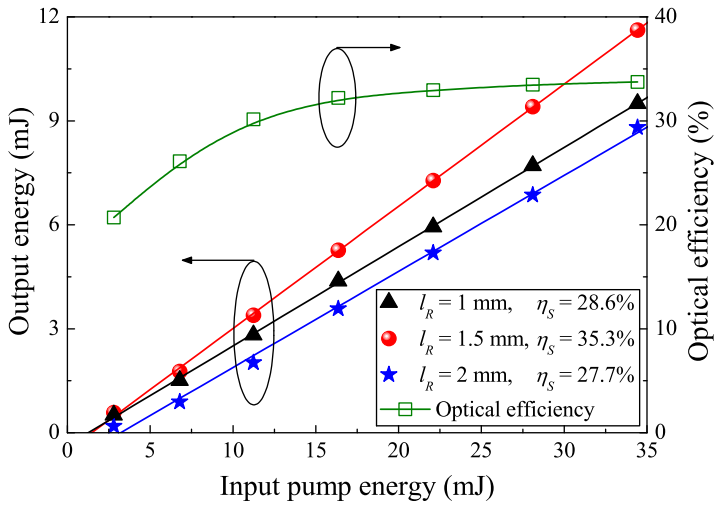


**Figure 3.** Output energy of Yb:YAG/$YVO_4$ RMLs with three different $l_R$s and optical efficiency of Yb:YAG/$YVO_4$ RMLs with $l_R$ = 1.5 mm versus the input pump energy.

Figure 3 depicts the output energy of QCW laser-diode pumped Yb:YAG/$YVO_4$ RMLs with three $l_R$s as a function of input pump energy ($E_{in} = P_{in} \times t_p$). The threshold pump energies for Yb:YAG/$YVO_4$ RMLs with $l_R$ = 1, 1.5 and 2 mm were measured to be 2.6, 2.5 and 2.6 mJ, respectively. The laser output energy increases linearly with $E_{in}$ for three Yb:YAG/$YVO_4$ RMLs. Efficient laser performance was achieved for three Yb:YAG/$YVO_4$ RMLs consisting $YVO_4$ Raman crystals with different thicknesses. The slope efficiency was approximately 28.6%, 35.3% and 27.7% for Yb:YAG/$YVO_4$ RML with $l_R$ = 1, 1.5 and 2 mm, respectively. The best laser performance was observed in Yb:YAG/$YVO_4$ RML with 1.5 mm thick $YVO_4$ crystal. The highest output laser energy of 11.6 mJ was achieved in the Yb:YAG/$YVO_4$ RML with $l_R$ = 1.5 mm at $E_{in}$ = 34.4 mJ. The optical efficiency was as high as 34%, which was two times of that obtained in the CW laser-diode pumped Yb:YAG/$YVO_4$ RML [35]. This was attributed to high pump power intensity and alleviated thermal effect achieved with QCW laser-diode pumping. No rollover was observed for the output energy in the Yb:YAG/$YVO_4$ RMLs. Therefore, the output energy can be further scaled in the Yb:YAG/$YVO_4$ RMLs by applying high pump energy.

By taking account into the effective overlap between fundamental and Stokes fields, $A_e$, the pump power at intracavity Raman laser threshold, $P_{th}$, can be calculated theoretically [16],

$$P_{th} = \frac{(T_S + L_S) L_F}{4 l_R} \frac{\lambda_F}{\lambda_P} \frac{A_e}{g_e} \frac{1}{1 - e^{-\alpha l}} \tag{1}$$

**Table 2.** Parameters used in theoretical calculation of threshold pump power of Raman lasers.

| Parameter | Symbol | Value |
|---|---|---|
| Absorption coefficient of Yb:YAG crystal | $\alpha$ ($cm^{-1}$) | 15 |
| Length of Yb:YAG crystal | $L$ (mm) | 1.2 |
| Effective Raman gain coefficient at 259 $cm^{-1}$ | $g_e$ (cm/GW) | 1.1 |
| Pump laser wavelength | $\lambda_P$ (nm) | 940 |
| Fundamental laser wavelength | $\lambda_F$ (nm) | 1050 |
| Beam waist | $w_F$ ($\mu$m) | 80 |
| Total round-trip loss for fundamental field | $L_F$ (%) | 0.2 |
| Mirror transmission for Stokes field | $T_S$ (%) | 0.4 |
| Total round-trip loss for Stokes field | $L_S$ (%) | $l_R = 1$ mm: 0.4<br>$l_R = 1.5$ mm: 0.55<br>$l_R = 2$ mm: 0.7 |

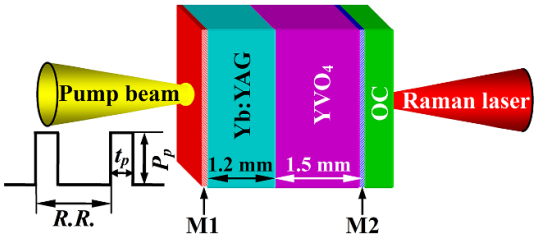


**Figure 4.** Schematic diagram for a QCW laser diode pumped Yb:YAG/$YVO_4$ coupled-RML. M1 is the rear cavity mirror, M2 is the front cavity mirror, OC is the extra output coupler with partial reflectivity of 60%. $t_p$, $P_p$, and *R.R.* are the pulse duration, pump power and repetition rate of QCW laser diode, respectively.

$$A_e = \frac{1}{\int_{-\infty}^{\infty}\int_{-\infty}^{\infty} I_S(x,y)\, I_F(x,y)\, dxdy} \tag{2}$$

where $I_F(x,y)$ and $I_S(x,y)$ are the normalized fundamental and Stokes laser intensity distribution

From equation (1), it can be seen that the threshold pump power of intracavity Raman laser is proportional to loss and inversely proportional to Raman crystal length ($l_R$). Both Raman gain and loss increase with $l_R$. Therefore, there is an optimized Raman crystal length for achieving lowest threshold pump power in Yb:YAG/$YVO_4$ RML. With the parameters listed in table 2, the threshold pump powers of Yb:YAG/$YVO_4$ RML with different $l_R$s were theoretically calculated to be 2.4 W, 2.26 W and 2.3 W. The theoretically calculated $l_R$-dependent threshold pump powers are in good agreement with the SRS threshold pump powers measured experimentally in the Yb:YAG/$YVO_4$ RML with different $l_R$s.

### 3.2. Coupled Yb:YAG/$YVO_4$ RML

A plane-parallel mirror with partially reflection of 60% was attached tightly to the $YVO_4$ output surface to form Yb:YAG/$YVO_4$ coupled Raman laser cavity for expanding the laser spectral range. The Yb:YAG laser medium, $YVO_4$ Raman gain medium and partially reflected mirror (OC) were held together to construct coupled-RML. The schematic of the coupled-RML with 1.5 mm thick $YVO_4$ crystal as Raman gain medium is shown in figure 4.

Figure 5 shows the measured laser spectra of Yb:YAG/$YVO_4$ coupled-RML with $l_R = 1.5$ mm at different incident pump powers. At different $P_{in}$s, laser spectra of Yb:YAG/$YVO_4$ coupled-RML are totally different from those of Yb:YAG/$YVO_4$ RML, as shown in figure 2(b). At $P_{in} = 3.1$ W, the Yb:YAG/$YVO_4$ coupled-RML oscillated at two wavelengths (1030 nm and 1050 nm), no Raman laser was observed, which was different from the lasers oscillating at 1050 nm and 1079 nm in the Yb:YAG/$YVO_4$ RML. Further increasing $P_{in}$ up to 12.5 W, the first-order Stokes laser around 1079 nm and the second-order Stokes laser around 1110 nm were excited, as shown in figure 5(b), which was similar to that obtained in Yb:YAG/$YVO_4$ RML. However, the spectral bandwidths of the Raman lasers generated in the coupled-RML are wider than those obtained in the RML. With an extra output coupler to form Yb:YAG/$YVO_4$ coupled-RML, dramatical expansion of the Raman laser spectra has been achieved. Further increase in $P_{in}$, the laser spectral range at 1050 nm, 1079 nm and 1110 nm were further expanded, as shown in figures 5(c) and (d). The laser spectra at 1050 nm and 1079 nm connected together to form a broadband multi-longitudinal-mode laser spectrum at $P_{in} = 38.3$ W.

**Table 3.** Performance of Yb:YAG/$YVO_4$ coupled-RML and Yb:YAG/$YVO_4$ RML at $E_{in}$ = 34.4 mJ.

| | Yb:YAG/$YVO_4$ RML | Yb:YAG/$YVO_4$ coupled-RML |
|---|---|---|
| $E_{out}$, mJ | 11.6 | 4.3 |
| $\eta_{O-O}$, % | 34 | 12.4 |
| $\eta_S$, % | 35.3 | 12.6 |
| $\Delta\lambda$, nm | 11.7 + 22.4 | 55.4 |
| Mode number | 23 + 44 | 118 |

Notes: $E_{out}$ is output energy, $\eta_{O-O}$ is optical efficiency, $\eta_S$ is slope efficiency, $\Delta\lambda$ is spectral bandwidth.

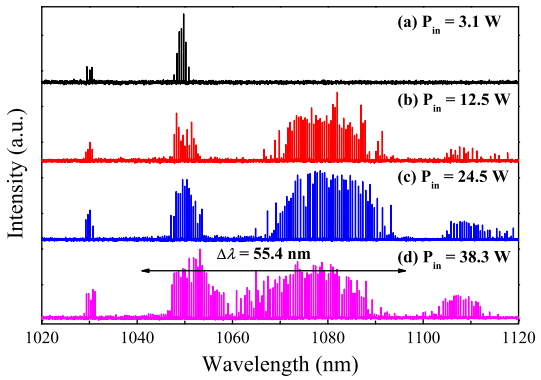


**Figure 5.** Evolution of the laser spectra with input pump power, (a) $P_{in}$ = 3.1 W, (b) $P_{in}$ = 12.5 W, (c) $P_{in}$ = 24.5 W, (d) $P_{in}$ = 38.3 W. The broadband multi-longitudinal-mode laser with bandwidth of 55.4 nm is achieved at $P_{in}$ = 38.3 W.

The broadband laser spectrum exhibits multiple longitudinal modes structure covering from 1041 nm to 1096.4 nm. The laser spectral range is as wide as 55.4 nm, which includes 118 longitudinal modes with typical mode separation of about 0.46 nm. The multi-longitudinal-mode laser spectral bandwidth of 55.4 nm obtained in the coupled-RML is 2 times of that obtained in the RML. This wide spectral bandwidth supports generation of Gaussian pulses with Fourier transform limited pulse duration of approximately 30 *f*s in mode-locked lasers. Table 3 gives the broadband multi-longitudinal-mode laser spectrum obtained in the coupled-RML at $P_{in}$ = 38.3 W, together with the laser spectrum obtained in the RML for comparison. The compact, broadband multi-longitudinal-mode coupled-RMLs could be potential laser sources for generating ultra-short laser pulses with self-mode-locking. Dramatically expansion of the bandwidth of the multi-longitudinal-mode laser in the coupled-RML is attributed to the frequency-dependent variable transmission of output coupler. Therefore, the output coupling losses for the fundamental, Raman lasers are dynamically adjusted for achieving broadband multi-longitudinal-mode laser spectrum in coupled-RML.

Figure 6 depicts the variation of the output energy and optical efficiency with the input pump energy for the coupled-RML, together with the laser performance of the RML. The threshold incident pump energy for lasing in coupled-RML is nearly the same as that for the RML. The output energy increases linearly with $E_{in}$, and slope efficiency is 12.6%. The maximum output energy was 4.3 mJ at $E_{in}$ = 34.4 mJ. The optical efficiency was 12.4%. The optical efficiency of 10.7% at $E_{in}$ = 2.8 mJ increases slightly to 13.2% at $E_{in}$ = 11.2 mJ. Further increase in $E_{in}$, the optical efficiency decreases slightly. The optical efficiency of 13.2% at $E_{in}$ = 11.2 mJ drops slightly to 12.4% at $E_{in}$ = 34.4 mJ. There is 6% difference for the optical efficiency when $E_{in}$ increases from 11.2 mJ to 34.4 mJ. There is an optimal $E_{in}$ for achieving highest optical efficiency in Yb:YAG/$YVO_4$ coupled-RML. The optical efficiency of over 10% has been achieved in the whole pump energy region. The slight variation of the optical efficiency with $E_{in}$ in the coupled-RML clearly shows that the conversion from multi-longitudinal-mode fundamental lasers to multi-longitudinal-mode Raman lasers is effective and less sensitive to the pump energy induced thermal effect.

Compared to the laser spectrum and output energy obtained in the RML, the output energy is low and the optical efficiency is sacrificed in the coupled-RML, however, the broadband multi-longitudinal-mode laser is achieved by dynamically adjusting losses of the fundamental and Stokes lasers. The optical efficiency of the coupled-RML can be further improved by adjusting the reflectivity of the external output coupler. Therefore, coupled-RML should be a potential laser for generating efficient broadband multi-longitudinal-mode laser.

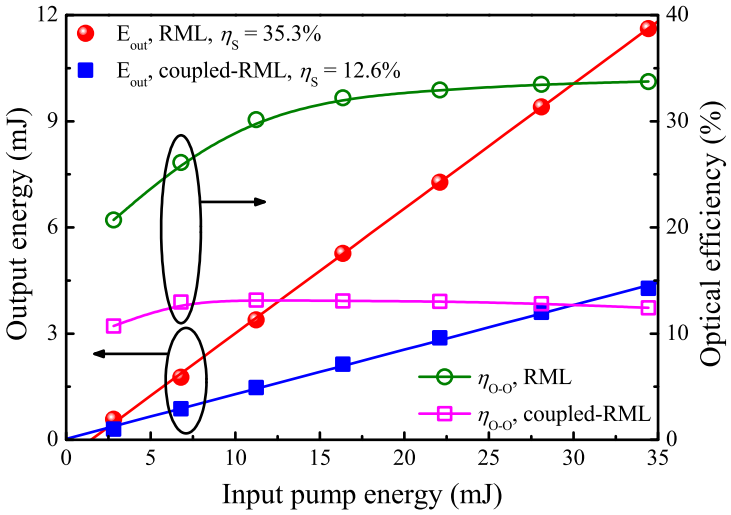


**Figure 6.** Output energy and optical efficiency of Yb:YAG/$YVO_4$ coupled-RML with $l_R = 1.5$ mm versus the input pump energy. Output energy and optical efficiency of Yb:YAG/$YVO_4$ RML with $l_R = 1.5$ mm as a function of the input pump energy is given for comparison.

## 4. Theoretical modelling

For the Yb:YAG/$YVO_4$ coupled-RML with an external Fabry–Perot (FP) output coupler, the spectral transmission is given as follows [34],

$$T_{FP}(\nu) = \frac{(1-R_{OC})(1-R_E)}{\left(1-\sqrt{R_{OC}R_E}\right)^2 + 4\sqrt{R_{OC}R_E}\left[sin\left(\frac{\pi\nu}{\Delta\nu}\frac{L_E}{L_C^*}\right)\right]^2} \tag{3}$$

where $R_{OC}$ and $R_E$ are the reflectivity of the coatings on the $YVO_4$ crystal and the external plane-parallel mirror, respectively. $L_E$ is the distance between the output surface of the $YVO_4$ crystal and external plane-parallel mirror, $L_C^*$ is the optical length of the RML cavity, $\Delta\nu = c/2L_C^*$, is the separation between two adjacent longitudinal modes in the RML cavity, $c$ is the speed of light in vacuum.

For plane-parallel Yb:YAG/$YVO_4$ coupled-RML, the frequency spectrum within an external FP cavity can be expressed as

$$I_F(\nu) = T_{FP}(\nu) I_0(\nu) \tag{4}$$

where $I_0(\nu)$ is the possible resonator longitudinal modes oscillating in the Yb:YAG/$YVO_4$ RML. Based on the damped harmonic oscillator, $I_0(\nu)$ can be expressed with an analytical form as follows,

$$I_0(\nu) = \sum_{n=-N}^{N} \frac{A_n \gamma \nu^2}{\left[\nu^2 - (\nu_0 + n\Delta\nu)^2\right]^2 + (\gamma\nu)^2} \tag{5}$$

where $A_n$ is the weighting coefficient of the longitudinal mode, $\nu_0$ is the central wavelength, $\gamma$ is the linewidth of the lasing mode. It is reasonable to assume that the gain profiles centered at 1030 nm or 1050 nm in Yb:YAG crystal can be treated as a Lorenz distribution.

It is reasonable to assume that the wavelength conversion is generally homogeneous for each lasing mode in a damped harmonic oscillator. Therefore, the frequency spectrum formed by a fundamental laser through SRS effect for the Yb:YAG/$YVO_4$ coupled-RML including cascade Stokes emissions can be expressed as,

$$I_R(\nu) = \left(1 - \sum_{m=1}^{M} \eta_m\right) I_F(\nu) + \sum_{m=1}^{M} \eta_m I_F(\nu + m\nu_R) \tag{6}$$

where $\eta_m$ is the conversion efficiency of the $m$th-order Stokes emission, $\nu_R$ is the Raman shift frequency. Therefore, the total frequency spectrum generated through different Raman shift lines in a Yb:YAG/$YVO_4$ coupled-RML can be expressed as

$$I_T(\nu) = I_{R1}(\nu) + I_{R2}(\nu) \tag{7}$$

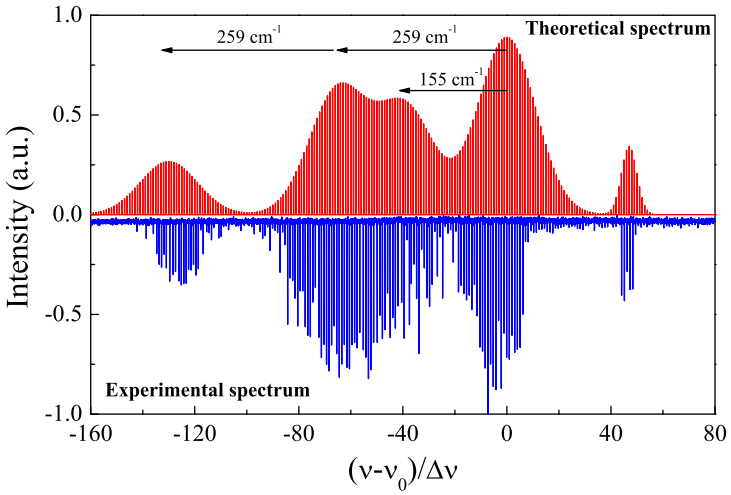


**Figure 7.** Theoretically calculated frequency spectrum of Yb:YAG/$YVO_4$ coupled-RML, which is formed by the Raman lasers converted from fundamental laser at 1050 nm with 259 $cm^{-1}$ and 155 $cm^{-1}$ Raman shift lines of $YVO_4$ crystal. The experimentally obtained frequency spectrum at $P_{in} = 38.3$ W is displayed as mirror image for comparison.

where $I_{R1}(\nu)$ and $I_{R2}(\nu)$ are the frequency spectrum of the Yb:YAG/$YVO_4$ coupled-RML through Raman shift lines 259 $cm^{-1}$ and 155 $cm^{-1}$, respectively.

A MATLAB software was used to carry out the theoretical simulation of frequency spectrum formed with cascade stimulated Raman scattering effect in Yb:YAG/$YVO_4$ coupled-RML. The Raman laser conversion efficiencies for different fundamental lasers were taken from the output energies at different incident pump energies.

Figure 7 shows the calculated multi-longitudinal-mode laser frequency spectrum in the Yb:YAG/$YVO_4$ coupled-RML. The broadband multi-longitudinal-mode laser frequency spectrum is formed by the Raman lasers converted from fundamental laser at 1050 nm with 259 $cm^{-1}$ and 155 $cm^{-1}$ Raman shift lines of $YVO_4$ crystal, together with the fundamental lasers at 1050 nm and 1030 nm. The parameters used in the calculations are $\Delta\nu = 29.57$ GHz, $A_n = \exp(-n^2/2\sigma^2)$, $\sigma = 10$, $N = 44$, $\gamma = 10$ kHz, $L_E = 0$, $\nu_{R1} = 7.77$ THz (for 259 $cm^{-1}$), $\nu_{R2} = 4.65$ THz (for 155 $cm^{-1}$), $\eta_1 = 0.35$, $\eta_2 = 0.15$. The experimental parameters used in the calculation are associated with the Yb:YAG/$YVO_4$ coupled-RML, such as $R_{OC} = 0.995$ for 1050 nm and $R_{OC} = 0.994$ for 1030 nm, $R_E = 0.6$. The theoretically calculated frequency spectrum provides a solid evidence that the broadband multi-longitudinal-mode laser spectrum in Yb:YAG/$YVO_4$ coupled-RML has been achieved through Raman conversion from the fundamental laser at 1050 nm by utilizing the 259 $cm^{-1}$ and 155 $cm^{-1}$ Raman shift lines. The experimentally obtained laser spectrum is in good agreement with the theoretically calculated frequency spectrum, as shown in figure 7. Some discrepancies between the theoretical result and experimental result are attributed to the neglection of the mode competition between Raman conversion in the theoretical calculation.

## 5. Conclusions

In conclusion, efficient Raman laser oscillating in broadband multi-longitudinal modes has been generated in Yb:YAG/$YVO_4$ RMLs under QCW laser-diode pumping. The output energy was 11.6 mJ at input pump energy of 33.4 mJ. The optical efficiency of as high as 34% was achieved. Multi-longitudinal-mode Raman laser centered at 1079 nm with bandwidth of 22.4 nm has been obtained in the RML with $l_R = 1.5$ mm. The broadband multi-longitudinal-mode laser has been achieved in the Yb:YAG/$YVO_4$ coupled-RML formed with an external FP partially reflective mirror. The bandwidth of the broadband multi-longitudinal-mode laser spectrum is 55.4 nm covering from 1041 nm to 1096.4 nm and including 118 equidistant longitudinal modes. Maximum output energy of the broadband laser was 4.3 mJ at $E_{in} = 33.4$ mJ. The optical efficiency was 12.4% for Yb:YAG/$YVO_4$ coupled-RML. Formation of broadband multi-longitudinal-mode laser in the coupled-RML is attributed to the dynamically modulating the frequency-dependent transmission of the output coupler through the cascade Raman conversion process. For the coupled-RML, two Raman shift lines (259 $cm^{-1}$ and 155 $cm^{-1}$) of $YVO_4$ crystal were utilized for cascade Raman conversion from the 1050 nm fundamental laser to generate broadband multi-longitudinal-mode laser. This work provides an effective and simple method to develop miniature solid-state Raman lasers for generating broadband multi-longitudinal-mode lasers.

## Acknowledgments

This work was supported by the National Natural Science Foundation of China (61275143, 61475130), the Program for New Century Excellent Talents in University (NCET-09-0669), and the Fundamental Research Funds for the Central Universities (20720192020).

## ORCID iD

Jun Dong https://orcid.org/0000-0001-7072-5435

## References

[1] Healy T, Gunning F C G and Ellis A D 2007 Multi-wavelength source using low drive-voltage amplitude modulators for optical communications *Opt. Express* **15** 2981–6
[2] He Y and Orr B J 2002 Rapidly swept, continuous-wave cavity ringdown spectroscopy with optical heterodyne detection: single- and multi-wavelength sensing of gases *Appl. Phys.* B **75** 267–80
[3] Weigl F 1971 A generalized technique of two-wavelength, nondiffuse holographic interferometry *Appl. Opt.* **10** 187–92
[4] Son S N, Song J J, Kang J U and Kim C S 2011 Simultaneous second harmonic generation of multiple wavelength laser outputs for medical sensing *Sensors* **11** 6125–30
[5] Farley R W and Dao P D 1995 Development of an intracavity-summed multiple-wavelength Nd:YAG laser for a rugged, solid-state sodium lidar system *Appl. Opt.* **34** 4269–73
[6] Okulov A Y 2020 Structured light entities, chaos and nonlocal maps *Chaos Solitons Fractals* **133** 109638
[7] Zhong K, Sun C L, Yao J Q, Xu D G, Xie X Y, Cao X L, Zhang Q L, Luo J Q, Sun D L and Yin S T 2013 Efficient continuous-wave 1053-nm Nd:GYSGG laser with passively Q-switched dual-wavelength operation for terahertz generation *IEEE J. Quantum Electron.* **49** 375–9
[8] Guo L *et al* 2010 1319 nm and 1338 nm dual-wavelength operation of LD end-pumped Nd:YAG ceramic laser *Opt. Express* **18** 9098–106
[9] Huang H T, He J L, Zhang B T, Yang K J, Zuo C H, Xu J L, Dong X L and Zhao S 2009 Intermittent oscillation of 1064 nm and 1342 nm obtained in a diode-pumped doubly passively Q-switched Nd:$YVO_4$laser *Appl. Phys.* B **96** 815–20
[10] Huang Y J, Tzeng Y S, Tang C Y, Chiang S Y, Liang H C and Chen Y F 2014 Efficient high-power terahertz beating in a dual-wavelength synchronously mode-locked laser with dual gain media *Opt. Lett.* **39** 1477–80
[11] Chu H W, Zhao J, Li Y F, Zhao S Z, Yang K J, Li T, Li D C, Li G D and Qiao W C 2016 Dual-wavelength Nd:LGGG laser intracavity pumped simultaneous OPO and SRS processes in single KTP *Appl. Opt.* **55** 1824–9
[12] Serrat C and Masoller C 2006 Modeling spatial effects in multi-longitudinal-mode semiconductor lasers *Phys. Rev.* A **73** 043812
[13] Dong J, Shirakawa A, Ueda K, Yagi H, Yanagitani T and Kaminskii A A 2006 Efficient $Yb^{3+}$:$Y_3Al_5O_{12}$ceramic microchip lasers *Appl. Phys. Lett.* **89** 091114
[14] Dong J, Shirakawa A, Ueda K, Xu J and Deng P Z 2006 Efficient laser oscillation of Yb:$Y_3Al_5O_{12}$single crystal grown by temperature gradient technique *Appl. Phys. Lett.* **88** 161115
[15] Demidovich A A, Grabtchikov A S, Lisinetskii V A, Burakevich V N, Orlovich V A and Kiefer W 2005 Continuous-wave Raman generation in a diode-pumped $Nd^{3+}$:$KGd(WO_4)_2$laser *Opt. Lett.* **30** 1701–3
[16] Spence D J 2015 Spatial and spectral effects in continuous-wave intracavity Raman lasers *IEEE J. Sel. Top. Quantum Electron.* **21** 1400108
[17] Lisinetskii V A, Grabtchikov A S, Demidovich A A, Burakevich V N, Orlovich V A and Titov A N 2007 Nd:KGW/KGW crystal: efficient medium for continuous-wave intracavity Raman generation *Appl. Phys.* B **88** 499–501
[18] Dekker P, Pask H M, Spence D J and Piper J A 2007 Continuous-wave, intracavity doubled, self-Raman laser operation in Nd:$GdVO_4$at 586.5 nm *Opt. Express* **15** 7038–46
[19] Bonner G M, Lin J, Kemp A J, Wang J, Zhang H, Spence D J and Pask H M 2014 Spectral broadening in continuous-wave intracavity Raman lasers *Opt. Express* **22** 7492–502
[20] Parrotta D C, Kemp A J, Dawson M D and Hastie J E 2013 Multiwatt, continuous-wave, tunable diamond Raman laser with intracavity frequency-doubling to the visible region *IEEE J. Sel. Top. Quantum Electron.* **19** 1400108
[21] Lee A J, Spence D J, Piper J A and Pask H M 2010 A wavelength-versatile, continuous-wave, self-Raman solid-state laser operating in the visible *Opt. Express* **18** 20013–8
[22] Dong J, Bass M, Mao Y L, Deng P Z and Gan F X 2003 Dependence of the $Yb^{3+}$ emission cross section and lifetime on temperature and concentration in yttrium aluminum garnet *J. Opt. Soc. Am.* B **20** 1975–9
[23] Lagatsky A A, Abdolvand A and Kuleshov N V 2000 Passive Q switching and self-frequency Raman conversion in a diode-pumped Yb:$KGd(WO_4)_2$laser *Opt. Lett.* **25** 616–8
[24] Grabtchikov A S, Kuzmin A N, Lisinetskii V A, Orlovich V A, Voitovich A P, Demidovich A A, Eichler H J and Titov A N 2003 Yb:KYW microchip laser with self-frequency Raman conversion *Quantum Electron.* **33** 165–7
[25] Kisel V E, Troshin A E, Tolstik N A, Shcherbitsky V G, Kuleshov N V, Matrosov V N, Matrosova T A and Kupchenko M I 2005 Q-switched $Yb^{3+}$:$YVO_4$laser with Raman self-conversion *Appl. Phys.* B **80** 471–3
[26] Jiang W, Zhu S, Chen W, Lin H, Liu Y, Chen Z, Zhang G, Chen Y, Duan Y and Chen Z 2015 Q-switched Yb:YAG/$YVO_4$Raman laser *IEEE Photonics Technol. Lett.* **27** 1080–3
[27] Jiang W, Li Z, Zhu S, Yin H, Chen Z, Zhang G and Chen W 2017 $YVO_4$ Raman laser pumped by a passively Q-switched Yb:YAG laser *Opt. Express* **25** 14033–42
[28] Wang X-L, Dong J, Wang X-J, Xu J, Ueda K-I and Kaminskii A A 2016 Multi-wavelength Yb:YAG/$Nd^{3+}$:$YVO_4$continuous-wave microchip Raman laser *Opt. Lett.* **41** 3559–62
[29] Lee C Y, Chang C C, Liang H C and Chen Y F 2014 Frequency comb expansion in a monolithic self-mode-locked laser concurrent with stimulated Raman scattering *Laser Photon. Rev.* **8** 750–5
[30] Guo B, Wang S H, Wu Z X, Wang Z X, Wang D H, Huang H, Zhang F, Ge Y Q and Zhang H 2018 Sub-200 fs soliton mode-locked fiber laser based on bismuthene saturable absorber *Opt. Express* **26** 22750–60

[31] Yan P G, Lin R Y, Chen H, Zhang H, Liu A J, Yang H P and Ruan S C 2015 Topological insulator solution filled in photonic crystal fiber for passive mode-locked fiber laser *IEEE Photonics Technol. Lett.* **27** 264–7
[32] Liu J, Chen Y, Tang P H, Xu C W, Zhao C J, Zhang H and Wen S C 2015 Generation and evolution of mode-locked noise-like square-wave pulses in a large-anomalous-dispersion Er-doped ring fiber laser *Opt. Express* **23** 6418–27
[33] Liang W, Ilchenko V S, Savchenkov A A, Matsko A B, Seidel D and Maleki L 2010 Passively mode-locked Raman laser *Phys. Rev. Lett.* **105** 143903
[34] Chang M T, Huang T L, Liang H C, Su K W and Chen Y F 2017 Broad expansion of optical frequency combs by self-Raman scattering in coupled-cavity self-mode-locked monolithic lasers *Opt. Express* **25** 7627–36
[35] Dong J, Wang X L, Zhang M M, Wang X J and He H S 2018 Structured optical vortices with broadband comb-like optical spectra in Yb:$Y_3Al_5O_{12}$/$YVO_4$Raman microchip laser *Appl. Phys. Lett.* **112** 161108
[36] Dong J and Ueda K 2005 Temperature-tuning Yb:YAG microchip lasers *Laser Phys. Lett.* **2** 429–36